

Article

Surface Reconstruction of Cobalt-Based Polyoxometalate and CNT Fiber Composite for Efficient Oxygen Evolution Reaction

Irsa Tariq ^{1,†}, Muhammad Adeel Asghar ^{1,†}, Abid Ali ^{2,*}, Amin Badshah ^{1,3}, Syed Mustansar Abbas ⁴, Waheed Iqbal ¹, Muhammad Zubair ¹, Ali Haider ^{1,3,*} and Shahid Zaman ^{5,*}

¹ Department of Chemistry, Quaid-i-Azam University, Islamabad 45320, Pakistan

² Department of Chemistry, The University of Lahore, Lahore 54590, Pakistan

³ Pakistan Academy of Science, 3-Constitution Avenue Sector G-5/2, Islamabad 44000, Pakistan

⁴ Nanoscience and Technology Department, National Centre for Physics, Quaid-i-Azam University Campus, Islamabad 45320, Pakistan

⁵ Key Laboratory of Energy Conversion and Storage Technologies, Southern University of Science and Technology, Shenzhen 518055, China

* Correspondence: abid.ali@chem.uol.edu.pk (A.A.); ahaider@qau.edu.pk (A.H.); shahid@sustech.edu.cn (S.Z.); Tel.: +92-3215051352 (A.A.); +92-5190642132 (A.H.); +86-18033400557 (S.Z.)

† These authors contributed equally to this work.

Abstract: Polyoxometalates (POMs), as carbon-free metal-oxo-clusters with unique structural properties, are emerging water-splitting electrocatalysts. Herein, we explore the development of cobalt-containing polyoxometalate immobilized over the carbon nanotube fiber (CNTF) (Co₄POM@CNTF) towards efficient electrochemical oxygen evolution reaction (OER). CNTF serves as an excellent electron mediator and highly conductive support, while the self-activation of the part of Co₄POM through restructuring in basic media generates cobalt oxides and/or hydroxides that serve as catalytic sites for OER. A modified electrode fabricated through the drop-casting method followed by thermal treatment showed higher OER activity and enhanced stability in alkaline media. Furthermore, advanced physical characterization and electrochemical results demonstrate efficient charge transfer kinetics and high OER performance in terms of low overpotential, small Tafel slope, and good stability over an extended reaction time. The significantly high activity and stability achieved can be ascribed to the efficient electron transfer and highly electrochemically active surface area (ECSA) of the self-activated electrocatalyst immobilized over the highly conductive CNTF. This research is expected to pave the way for developing POM-based electrocatalysts for oxygen electrocatalysis.

Keywords: polyoxometalates; carbon nanotube fibers; oxygen evolution reaction; water oxidation; electrocatalysis



Citation: Tariq, I.; Asghar, M.A.; Ali, A.; Badshah, A.; Abbas, S.M.; Iqbal, W.; Zubair, M.; Haider, A.; Zaman, S. Surface Reconstruction of Cobalt-Based Polyoxometalate and CNT Fiber Composite for Efficient Oxygen Evolution Reaction. *Catalysts* **2022**, *12*, 1242. <https://doi.org/10.3390/catal12101242>

Academic Editor: Carlo Santoro

Received: 18 September 2022

Accepted: 13 October 2022

Published: 15 October 2022

Publisher's Note: MDPI stays neutral with regard to jurisdictional claims in published maps and institutional affiliations.



Copyright: © 2022 by the authors. Licensee MDPI, Basel, Switzerland. This article is an open access article distributed under the terms and conditions of the Creative Commons Attribution (CC BY) license (<https://creativecommons.org/licenses/by/4.0/>).

1. Introduction

The production of renewable and clean energy is one of the most critical issues of the modern sustainable society. Therefore, the development of green and sustainable energy science by means of energy conversion and storage technologies is of utmost importance [1–5]. Water is the essential renewable energy source that has the potential to meet current energy needs by producing hydrogen as green fuel through photochemical, electrochemical, or photoelectrochemical processes [6,7]. In electrochemical water splitting, water electrolysis generates hydrogen and oxygen at the cathode and anode, respectively. Water oxidation into molecular oxygen is a more challenging half reaction due to the four-proton and four-electron transfer multistep process as opposed to the two-electron and two-proton hydrogen evolution reaction (HER) [8]. Therefore, there is a need to develop efficient water oxidation electrocatalysts to overcome their sluggish kinetics and large overpotential [9].

Rare earth metal-oxide-based electrocatalysts, such as ruthenium and iridium oxides, demonstrated high water oxidation efficiency in both acidic and basic environments [10]. However, their scarcity and high cost prevent their usage on a commercial basis. Over the past few years, Earth-abundant transition metal oxides [11–14], phosphides and sulfides [15,16], selenides [17], perovskites [18], olivines [19], hydro(oxy)oxides [20,21] and chalcogenides [22] have been promising photochemical and electrochemical water oxidation catalysts.

Polyoxometalates (POMs), also known as polyoxoanions, are polynuclear oxo-bridged anionic clusters of early transition metals in their highest oxidation states, and exhibit a wide range of structural and compositional characteristics [23]. They are used extensively in catalysis, medicine, electrochemistry, photochromism, and magnetism [24]. In 2008, the noble metal-based POM, i.e., $[\text{Ru}_4\text{O}_4(\text{OH})_2(\text{H}_2\text{O})_4(\text{SiW}_{10}\text{O}_{36})_2]^{10-}$ was independently the first example of an efficient water oxidation catalyst by the group of Bonchio [25] and Hill [26]. Soon after the demonstration of Ru-based POM, research was further extended towards cheap metals-based electrocatalysts [27–29]. Of all known POM-based frameworks, the tetracobalt(II)-containing Weakly dimer, i.e., $[\text{Co}_4(\text{H}_2\text{O})_2(\text{PW}_9\text{O}_{34})_2]^{10-}$ (Co_4), which was identified by Weakly in 1973 [30], is widely used as electrocatalyst for oxygen evolution reaction (OER) [31–46]. In 2011, Stracke et al. reported the same catalyst for water oxidation and indicated that the dominant water oxidation catalyst was heterogeneous CoO_x rather than homogenous Co_4 in basic media [33]. Later, in 2013, Vickers et al. confirmed that Co_4 -POM is a true molecular water oxidation catalyst by differentiating homogenous and heterogeneous water oxidation catalysts [36]. Till now, POM immobilized over different substrates was utilized as an electrocatalyst for OER activity due to its reversible stepwise multielectron transfer ability [28,46]. Furthermore, photo- and electrocatalytic performance was investigated and understood at the molecular level for POMs immobilized over conducting materials such as graphene, carbon nanotubes (CNTs), and graphitic carbon nitride (gC_3N_4), which reveals changes in the electrical structure of the cluster and some cases of self-activation through the restructuring that takes place depending upon the pH of the medium [31–47].

Carbon nanotube fibers (CNTFs) are an essential class of conducting materials composed of arrays of CNTs aligned in one dimension [48,49]. These are quasi-one-dimensional assemblies having unique characteristics such as high stiffness and tensile strength, low weight, excellent mechanical and electrical properties, high chemical resistance, high aspect ratio with low defects, self-lubrication and corrosion resistance, high-temperature tolerance, and high electrical conductivity [48,49]. CNTF improves electrical conductivity by increasing the charge carrier density in a fibrous carbon conjugated system.

Motivated by the electrocatalytic activity of Co_4 -POMs, and the exceptional properties, including excellent mechanical and electrical, high chemical resistance, and high surface area of CNTFs, we present a 4-Co(II)-based tungstophosphate immobilized on CNTF ($\text{Co}_4\text{POM@CNTF}$) as an efficient water oxidation catalyst in alkaline medium. Self-activated electrocatalyst showed efficient activity for water oxidation with a low overpotential of 323 mV at a current density of 10 mA cm^{-2} and Tafel slope of 69 mV dec^{-1} . Chronoamperometry over an extended time showed the stability and robustness of the self-activated $\text{Co}_4\text{POM@CNTF}$.

2. Results and Discussion

2.1. Characterization

The morphological features of bare CNTF and $\text{Co}_4\text{POM@CNTF}$ were investigated through SEM analysis. Figure 1a,b show the SEM images of bare CNTF at different magnifications. The SEM images of $\text{Co}_4\text{POM@CNTF}$ show that Co_4POM was uniformly distributed on the surface of CNTFs (Figure 1c,d).

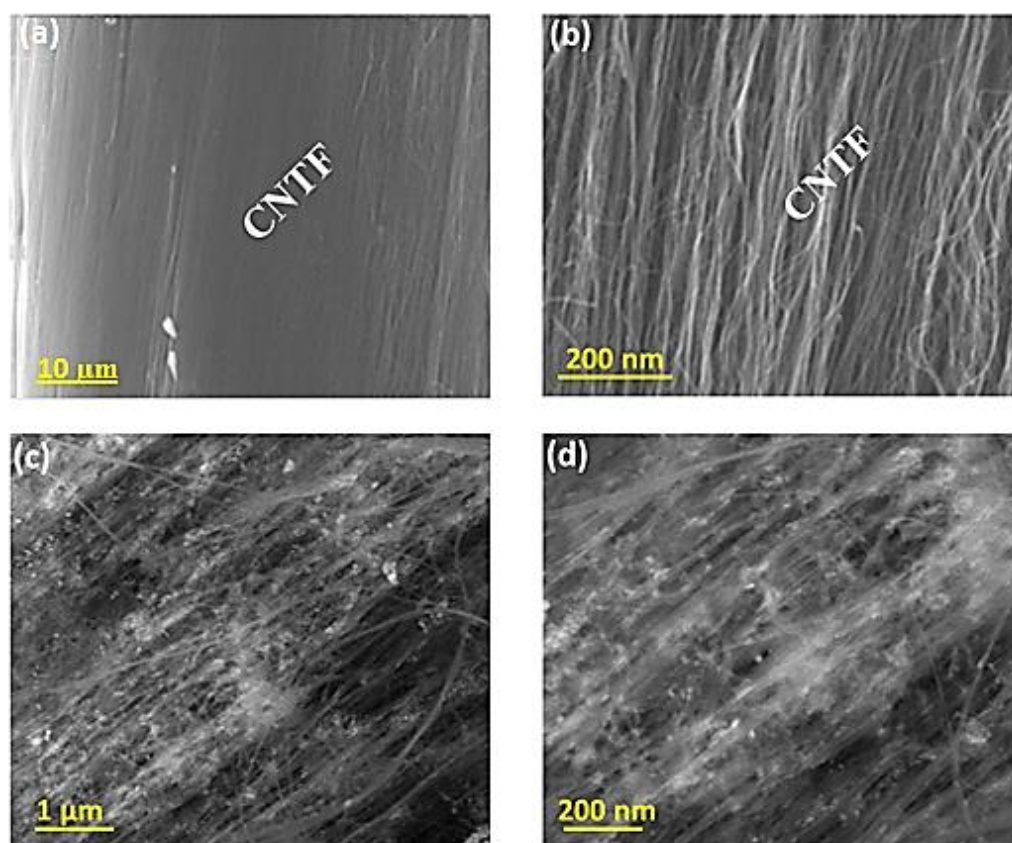


Figure 1. SEM images of (a,b) bare CNTF and (c,d) Co₄POM@CNTF at different magnifications.

Furthermore, Co₄POM@CNTF was characterized through energy-dispersive X-ray (EDX) spectroscopy to identify its elemental composition. Figure 2a shows that cobalt (Co), tungsten (W), phosphorus (P), oxygen (O), potassium (K) and sodium (Na) were all present in the modified electrode that stemmed from Co₄POM. A peak observed in the range from 0.1 to 0.2 keV was assigned to carbon, which is attributed to the CNTF substrate. The peak between 6.2 and 6.6 keV was of iron (Fe) and arose because of the iron catalyst used for the synthesis of CNTF through chemical vapor deposition (CVD) method [50]. Figure 2b illustrates the EDX-layered image depicting that all the components (colored dots) of Co₄POM were uniformly spread throughout the surface of CNTF. Furthermore, elemental mapping supported the presence of the corresponding elements in the fabricated electrode (see Figure 2c).

The redox behavior of Co₄POM as a heterogeneous catalyst was examined and compared with that of bare CNTF. This further supports the successful immobilization of POM over CNTF (See Figure S1).

The fabricated electrode was characterized through X-ray diffraction analysis (XRD). Figure 3 shows that CNTF had an amorphous pattern, whereas that of Co₄POM@CNTF had prominent peaks at 6°, 8°, and 12° 2θ values, which confirmed the deposition of Co₄POM on the surface of CNTF. The peaks at 2θ values from 22° to 32° were not dominant due to the presence of the amorphous CNTF phase.

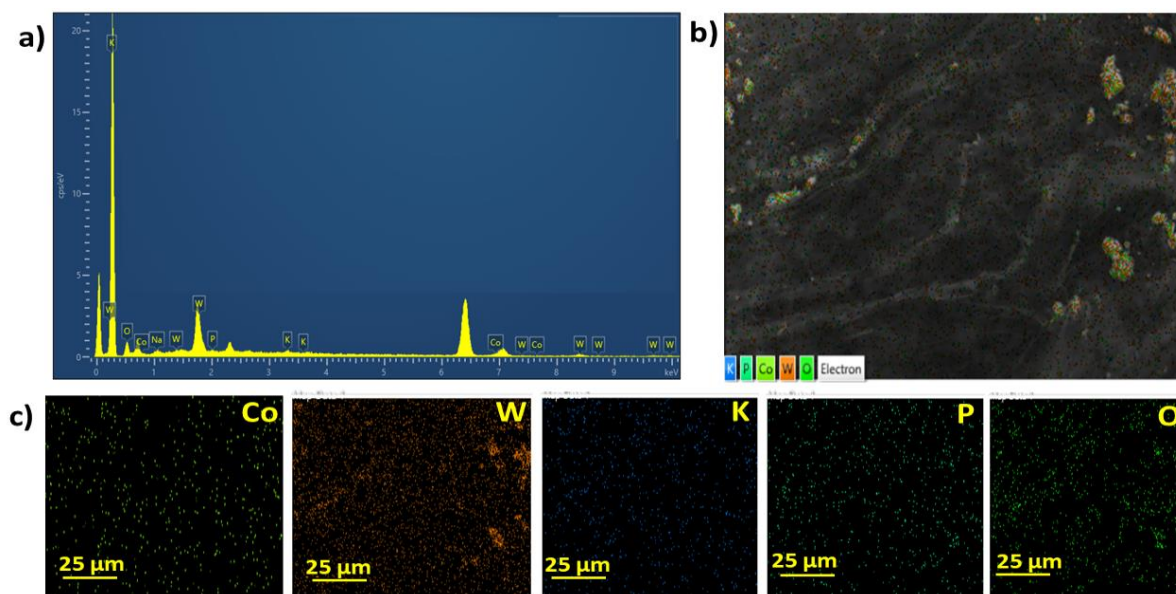


Figure 2. (a) EDX spectrum before catalytic activity, (b) elemental mapping layered image and (c) individual elements in $\text{Co}_4\text{POM@CNTF}$.

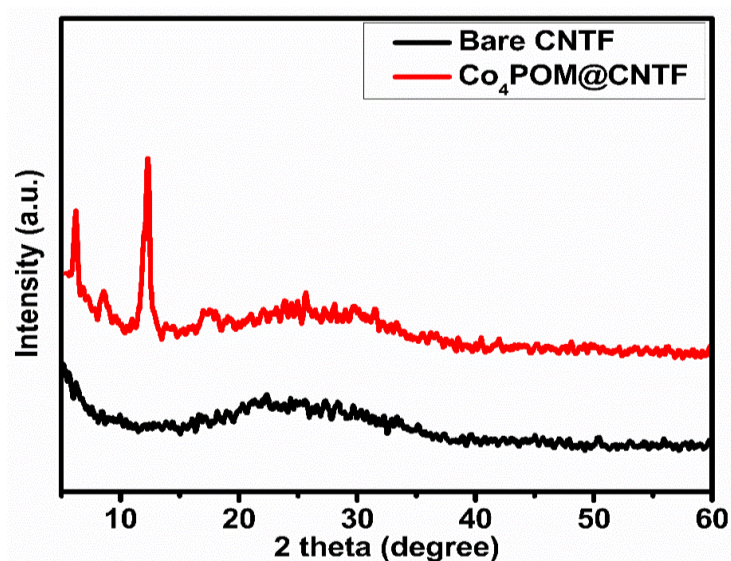


Figure 3. Overlaid XRD spectra of $\text{Co}_4\text{POM@CNTF}$ and bare CNTF.

2.2. Water Oxidation Studies

$\text{Co}_4\text{POM@CNTF}$ was employed as a working electrode to examine its OER activity in a three-electrode system at pH 13.5 (0.1 M KOH). By comparing the LSV curves of bare CNTF with the POM-modified electrode (Figure 4a), OER activity was significantly increased by the immobilization of Co_4POM over CNTF. $\text{Co}_4\text{POM@CNTF}$ demonstrated a remarkable increase in current density and significantly lower overpotential of 323 mV at anodic current density of 10 mA/cm^2 compared to the bare CNTF, which required overpotential of 737 mV for the same anodic current density. The low overpotential exhibited by the $\text{Co}_4\text{POM@CNTF}$ can be attributed to the tubular shape of CNTF that provided a high surface area and more active sites. Moreover, the high current-carrying capability and ballistic electron transport of CNTF increased electrical conductivity and current density due to its uniform nanochannels, which are superior to most of the Co-based heterogeneous electrocatalysts in basic media (Table S1) [51,52].

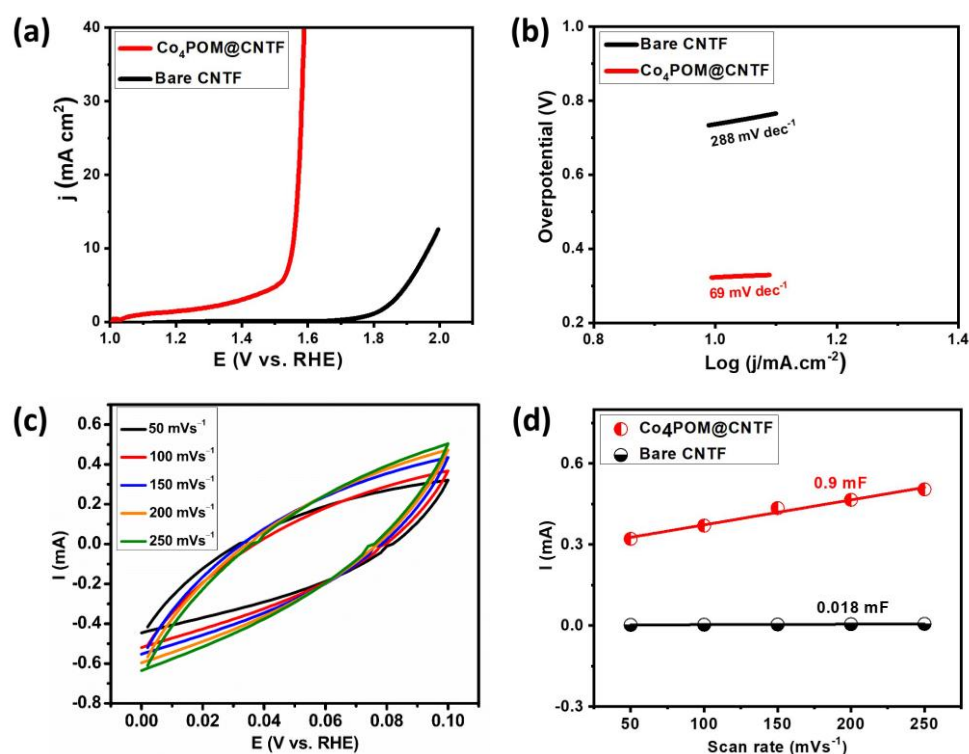


Figure 4. (a) LSV curves for CNTF and Co₄POM@CNTF in 0.1 M KOH at a scan rate of 10 mV s⁻¹; (b) Tafel plots for bare CNTF and Co₄POM@CNTF; (c) cyclic voltammograms for Co₄POM@CNTF at various scan rates from 50–250 mV/s; (d) scan rate versus current plots for the bare CNTF and Co₄POM@CNTF.

The Tafel plots of bare CNTF and as-prepared catalyst were constructed from the LSV curves, as shown in Figure 4b, to better understand the OER kinetics. Compared to the bare CNTF having a Tafel slope value of 288 mV/dec, Co₄POM@CNTF exhibited a Tafel slope value of 69 mV/dec, showing the enhanced reaction kinetics of the modified electrode. The faster rate of the multiple electron transfer process presented in Co₄POM@CNTF complimented the modified electrode's higher activity and current-carrying ability. The high activity of the modified electrode can be attributed to the self-activation of Co₄POM through restructuring in basic media that generated cobalt oxide and hydroxide as catalytic sites for OER. This self-activation, as a result of the restructuring of POM, was discussed in detail by the group of Streb [45]. Figures S2 and S3 show a similar phenomenon that aligned with the group's report. This was further supported by performing the UV-vis spectroscopy of Co₄POM in different pH solutions (see Figure S4) [33]. In 0.1 M phosphate buffer (pH 7), the absorption band at 582 nm depicted the presence of Co₄POM. In 1 M H₂SO₄ (pH 1), Co₄POM showed a slight hypsochromic shift due to protonation. On the other hand, in basic media (0.1 M KOH), Co₄POM showed multiple peaks, where the absorption peak at 628 nm indicated the presence of cobalt oxide and the restructuring of Co₄POM into CoOx. Furthermore, compared with the different classes of reported WOCs (Table S1), Co₄POM@CNTF showed excellent OER activity regarding overpotential and Tafel slope.

Figure 4c depicts the cyclic voltammograms at different scan rates, i.e., from 50 to 250 mVs⁻¹ in the non-Faradic region, to assess the ECSA of bare and Co₄POM-modified electrodes. The plot of anodic current versus scan rate at a potential from 0 to 0.1 V versus RHE, as illustrated in Figure 4d, yielded a straight line where the slope obtained with linear fitting showed the double-layer capacitance (C_{dl}) of the respective electrodes. By comparing the C_{dl} value of the bare CNTF with that of Co₄POM@CNTF, Co₄POM@CNTF

had a higher C_{dl} value of 0.9 mF owing to the higher surface area and thereby more active sites, resulting in higher efficiency. ECSA was calculated by applying Equation (1).

$$ECSA = C_{dl}/C_s, \quad (1)$$

where C_s represents the specific capacitance of the monolayer, and its value of 0.04 mF cm^{-2} was used for the calculation of ECSA [47]. ECSA is directly related to C_{dl} ; the higher the C_{dl} is, the higher the ECSA. Similarly, the roughness factor (R_f) is another surface characteristic and an important parameter for the electrocatalytic activity of the electrode material, and can be calculated with the ratio of ECSA and the geometric area of the electrode (equation given in Supplementary Materials.). The higher ECSA (22.5 cm^2) and R_f (402) calculated for $\text{Co}_4\text{POM@CNTF}$ than those for the bare CNTF (0.45 cm^2 and 8) confirm its improved electrochemical OER activity (see Table 1).

Table 1. Comparison of electrochemical parameters calculated for the bare CNTF and $\text{Co}_4\text{POM@CNTF}$ in alkaline media.

Electrocatalysts	η at 10 mA/cm^2 (mV)	Tafel Slope (mV dec^{-1})	C_{dl} (mF)	ECSA (cm^2)	R_f
Bare CNTF	737	288	0.018	0.45	8
$\text{Co}_4\text{POM@CNTF}$	323	69	0.9	22.5	402

To further understand the electrocatalytic activity of the catalyst, electrochemical impedance was performed to investigate the electron transport kinetics in bare and Co_4POM -modified CNTF electrodes. EIS was recorded in a frequency range from 0.1 to 105 Hz at a small AC amplitude of 5 mV. The Nyquist plot obtained with EIS presents the criterion for the efficient electrocatalyst having small charge transfer resistance in terms of the smaller diameter of the semicircle in the high-frequency region. In Figure 5a, the Nyquist plot of the real and imaginary components reveals that, for $\text{Co}_4\text{POM@CNTF}$, the semicircle had a smaller diameter than that of the bare CNTF owing to the smaller charge transfer resistance (R_{ct}) from the electrode. The calculated value for R_{ct} for $\text{Co}_4\text{POM@CNTF}$ was 2.533 kOhm, while that of the bare CNTF was 24.9 kOhm. This shows that, during OER, electron transport in the modified electrode is faster than that in the bare CNTF. This can be explained on the basis of the strong electrostatic interactions between CNTF and Co_4POM that boosted the transfer rates of electrons and thereby sped up electrocatalytic activity. These findings suggest that the synergistic effect of CNTF and Co_4POM contributed to the high electrocatalytic activity of the modified electrode towards OER.

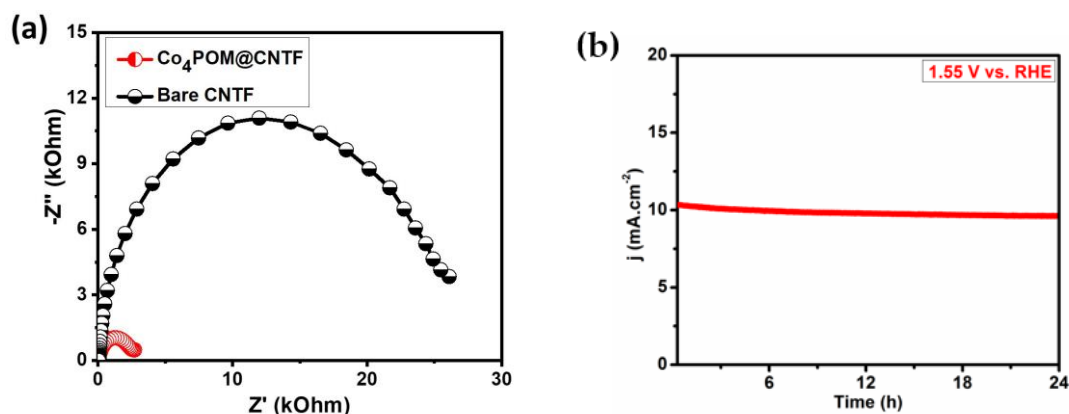


Figure 5. (a) Nyquist plot for the bare CNTF and $\text{Co}_4\text{POM@CNTF}$; (b) stability test for $\text{Co}_4\text{POM@CNTF}$ in 0.1 M KOH for 24 h at 1.55 V versus RHE.

Chronoamperometry was performed at 1.55 V vs. RHE for 24 h to examine the stability and robustness of Co₄POM@CNTF under constant oxygen production. Throughout the potentiostatic measurements, H₂ and O₂ bubbles continuously escaped out of the anode and cathode [53,54], respectively, and the catalyst generated current density of nearly 10 mA cm⁻² without any appreciable loss in activity (Figure 5b). On the basis of the chronoamperometric stability test, Co₄POM-modified electrode is a potential candidate electrocatalyst for OER that is stable for several hours.

Finding the Faradaic efficiency (FE) is an important experiment to support the catalyst's ability to produce oxygen during OER. FE is calculated by comparing the experimental and theoretical oxygen production during controlled-potential electrolysis (CPE). The CPE test was performed for 3000 s at 1.55 V against RHE in a 0.1 M KOH solution. To determine the experimentally calculated oxygen production, an oxygen probe of a dissolved oxygen (DO) meter was inserted into a gas-tight anodic portion during electrocatalytic activity. The theoretical yield of O₂ for a four-electron process was calculated using the charge built up during the electrochemical reaction (see Figure S5). On the basis of theoretical and actual yield calculations, the FE was approximately 94.9%.

Equations (2)–(5) represent the most likely mechanism of half reaction of water splitting as OER:



The proposed mechanism illustrates that the hydroxyl species (OH⁻) from water became attached to the catalyst by removing an electron to generate (Co₄POM@CNTF)/CoOx-OH^{*}, which was then combined with another OH⁻ to form oxospecies as surface-active sites. These active sites captured more OH⁻ ions to generate a hydroperoxide intermediate. Lastly, hydroperoxides produced O₂ molecules by reacting with OH⁻ in the solution. This is in line with the reports in the literature [55,56]. Table S1 shows the electrocatalytic activity of recently reported electrocatalysts, where it is evident that Co₄POM@CNTF showed appreciable electrocatalytic OER activity in comparison with that of other recently reported catalysts.

3. Experimental

3.1. Materials

The used chemicals were sodium tungstate dihydrate (Na₂WO₄·2H₂O), glacial acetic acid (CH₃COOH), cobalt acetate tetrahydrate (Co(CH₃COO)₂·4H₂O), disodium hydrogen phosphate heptahydrate (Na₂HPO₄·7H₂O), sodium chloride (NaCl), potassium hydroxide (KOH), potassium chloride (KCl), and ethanol (C₂H₅OH). All these chemicals were purchased from Sigma Aldrich and utilized without further purification.

3.2. Synthesis of Na₁₀[Co₄(H₂O)₂(PW₉O₃₄)₂] (Co₄POM)

Co₄POM was synthesized according to the procedure modified by Hill and coworkers [31], and was confirmed with FT-IR spectroscopy (see Figure S6). Briefly, 16.5 g of Na₂WO₄·2H₂O, 1.50 g Na₂HPO₄·7H₂O, and 3.2 g Co(CH₃COO)₂ were dissolved in 50 mL of distilled water, and the pH of this solution was adjusted to 7.8 with the addition of CH₃COOH. After that, the solution mixture was refluxed at 100 °C for 2 h, resulting in a dark purple solution. The solution was then saturated with NaCl and allowed to cool to room temperature. The obtained purple crystals were collected and recrystallized in hot water.

3.3. Electrode Fabrication

CNTF about 2.5 cm long was fixed onto a glass slide by binding both its ends with Teflon tape. A concentrated POM solution was drop-casted thrice onto CNTF with one hand, and the glass plate was dried in an oven at 70 °C. The fabricated electrode was then thermally treated at 120 °C for 72 h in a furnace followed by washing with water [57]. Lastly, the Teflon tape was removed from one end, which was sealed with conducting silver paste to produce the electrode connection. Figure 6 depicts electrode fabrication by drop casting.



Figure 6. Schematic illustration of electrode fabrication by drop casting.

3.4. Electrochemical Studies

The steady-state electrochemical measurements were carried out using a three-electrode setup at room temperature in a 0.1 M KOH solution (pH 13.5) as an electrolyte. The used working electrode was the modified CNTF (0.056 cm² surface area; calculations are in SI), whereas the reference and counter electrodes were an Ag/AgCl and platinum sheet electrode (2 × 6 mm), respectively. Linear sweep voltammetry (LSV), cyclic voltammetry (CV), chronoamperometry, and electrochemical impedance spectroscopy (EIS) tests were performed on a Gamry Interface 1010E potentiostat/galvanostat. All the measured potential values were converted into reversible hydrogen electrode (RHE) using the Nernst equation (E vs. RHE = 0.197 + $E_{\text{Ag/AgCl}} + 0.0591 \times \text{pH}$) and were iR -compensated. LSV was performed at a scan rate of 10 mV/s; to calculate the electrochemical surface area (ECSA), CV scans were performed at a scan rate from 50 to 250 mV/s in the non-Faradaic region. The chronoamperometric response was measured at 1.55 V vs. RHE for 24 h in an O₂-saturated KOH solution for the stability tests. The EIS was performed in the frequency range of 0.1–105 Hz at a small AC signal of 5 mV.

4. Conclusions

In conclusion, we reported the preparation of Co₄POM@CNTF via the drop-casting method followed by thermal treatment. The OER performance of the prepared electrocatalyst was improved significantly, in which CNTF served as an excellent electron mediator, while self-activated Co₄POM provided the catalytic sites. It exhibited low overpotential value, i.e., 323 mV, and faster kinetics for OER catalysis in terms of a smaller Tafel slope. The improvement in electrocatalytic performance may also be attributed to the increase in the high surface area of the catalyst; this was suggested by high ECSA to lead to high RF, providing more active sites. In a nutshell, the fabrication of POM over CNTF provides an efficient heterogeneous electrocatalyst with superior properties such as high activity, high surface area, and electron transfer ability for OER- and energy-related applications.

Supplementary Materials: The following supporting information can be downloaded at: <https://www.mdpi.com/article/10.3390/catal12101242/s1>. Figure S1: CV curves of bare CNTF and Co₄POM@CNTF in 0.1 M KOH at a scan rate of 10 mV s⁻¹; Figure S2: postcatalytic SEM images of Co₄POM@CNTF at (a) higher and (b) lower magnification; Figure S3: EDX spectrum of Co₄POM@CNTF after chronoamperometric stability test. Figure S4: UV-vis spectra of Co₄POM in different pH aqueous solutions; Figure S5: Faradic efficiency of Co₄POM@CNTF in 0.1M KOH at 1.55 V against RHE; Figure S6: FT-IR spectrum of synthesized Co₄POM. Table S1: comparative OER performance of Co-based heterogenous electrocatalysts in basic media. Equations: calculations of surface area of CNTF and RF. [45,47,58–66]

Author Contributions: Conceptualization, A.A. and A.H.; methodology, I.T., M.A.A. and A.A.; software, A.H.; validation, A.B. and A.H.; formal Analysis, S.M.A., W.I. and M.Z.; investigation, I.T., M.A.A., A.A., S.M.A. and A.H.; resources, A.B. and A.H.; data curation, A.H.; writing—original draft preparation, I.T., M.A.A., and A.A.; writing—review and editing, A.H. and S.Z.; visualization, I.T., M.A.A., A.A., S.Z. and A.H.; supervision, A.B. and A.H.; project administration, A.H.; funding acquisition, A.B. and A.H. All authors have read and agreed to the published version of the manuscript.

Funding: This research project was funded by PAS (2021-23) and HEC (20-14419/NRPU/R&D/HEC/2021).

Data Availability Statement: The data presented in this study is available in Supplementary Material.

Acknowledgments: We are thankful to the Huisheng Peng group for providing CNT arrays. A.H. and A.B. are thankful to PAS for the financial support. A.H. is also thankful to HEC (20-14419/NRPU/R&D/HEC/2021) for the research project support.

Conflicts of Interest: The authors declare no competing interests.

References

1. Zaman, S.; Huang, L.; Douka, A.I.; Yang, H.; You, B.; Xia, B.Y. Oxygen reduction electrocatalysts toward practical fuel cells: Progress and perspectives. *Angew. Chem. Int. Ed.* **2021**, *60*, 17832–17852. [[CrossRef](#)] [[PubMed](#)]
2. Zaman, S.; Tian, X.; Su, Y.-Q.; Cai, W.; Yan, Y.; Qi, R.; Douka, A.I.; Chen, S.; You, B.; Liu, H.; et al. Direct integration of ultralow-platinum alloy into nanocarbon architectures for efficient oxygen reduction in fuel cells. *Sci. Bull.* **2021**, *66*, 2207–2216. [[CrossRef](#)]
3. Iftikhar, M.; Ali, B.; Nisar, T.; Wagner, V.; Haider, A.; Rehman, A.; Hussain, S.; Bahadar, A.; Saleem, M.; Abbas, S.M. Improving lithium-ion half/full cell performance of WO₃ protected SnO₂ core-shell nanoarchitectures. *ChemSusChem* **2021**, *14*, 917–928. [[CrossRef](#)]
4. Zaman, S.; Wang, M.; Liu, H.; Sun, F.; Yu, Y.; Shui, J.; Chen, M.; Wang, H. Carbon-based catalyst supports for oxygen reduction in proton-exchange membrane fuel cells. *Trends Chem.* **2022**, *5*, 886–906. [[CrossRef](#)]
5. Zaman, S.; Su, Y.Q.; Dong, C.L.; Qi, R.; Huang, L.; Qin, Y.; Huang, Y.C.; Li, F.M.; You, B.; Guo, W.; et al. Scalable molten salt synthesis of platinum alloys planted in metal-nitrogen-graphene for efficient oxygen reduction. *Angew. Chem. Int. Ed.* **2022**, *61*, 202115835–202115843. [[CrossRef](#)]
6. Li, J.; Triana, C.A.; Wan, W.; Saseendran, D.A.; Zhao, Y.; Balaghi, S.E.; Heidari, S.; Patzke, G.R. Molecular and heterogeneous water oxidation catalysts: Recent progress and joint perspectives. *Chem. Soc. Rev.* **2021**, *50*, 2444–2485. [[CrossRef](#)]
7. Ishaq, T.; Yousaf, M.; Bhatti, I.A.; Batool, A.; Asghar, M.A.; Mohsin, M.; Ahmad, M. A perspective on possible amendments in semiconductors for enhanced photocatalytic hydrogen generation by water splitting. *Int. J. Hydrogen Energy* **2021**, *46*, 39036–39057. [[CrossRef](#)]
8. Dau, H.; Limberg, C.; Reir, T.; Risch, M.; Roggan, S.; Strasser, P. The mechanism of water oxidation: From electrolysis via homogeneous to biological catalysis. *ChemCatChem* **2010**, *2*, 724–761. [[CrossRef](#)]
9. Favaro, M.; Yang, J.; Nappini, S.; Magnano, E.; Toma, F.M.; Crumlin, E.J.; Yano, J.; Sharp, I.D. Understanding the oxygen evolution reaction mechanism on CoO_x using operando ambient-pressure X-ray photoelectron spectroscopy. *J. Am. Chem. Soc.* **2017**, *139*, 8960–8970. [[CrossRef](#)]
10. Lyons, M.E.G.; Floquet, S. Mechanism of oxygen reactions at porous oxide electrodes. Part 2—Oxygen evolution at RuO₂, IrO₂ and Ir_xRu_{1-x}O₂ electrodes in aqueous acid and alkaline solution. *Phys. Chem. Chem. Phys.* **2011**, *13*, 5314–5335. [[CrossRef](#)]
11. Zhang, L.; Fan, Q.; Li, K.; Zhang, S.; Ma, X. First-row transition metal oxide oxygen evolution electrocatalysts: Regulation strategies and mechanistic understandings. *Sustain. Energy Fuels* **2020**, *4*, 5417–5432. [[CrossRef](#)]
12. Hong, W.T.; Risch, M.; Stoerzinger, K.A.; Grimaud, A.; Suntivich, J.; Shao-Horn, Y. Toward the rational design of non-precious transition metal oxides for oxygen electrocatalysis. *Energy Environ. Sci.* **2015**, *8*, 1404–1427. [[CrossRef](#)]
13. Mansoor, M.A.; Mazhar, M.; McKee, V.; Arifin, Z. Mn₂O₃-4TiO₂ semiconducting composite thin films for photoelectrochemical water splitting. *Polyhedron* **2014**, *75*, 135–140. [[CrossRef](#)]

14. Asghar, M.A.; Ali, A.; Haider, A.; Zaheer, M.; Nisar, T.; Wagner, V.; Akhter, Z. Electrochemically deposited amorphous cobalt-nickel-doped copper oxide as an efficient electrocatalyst toward water oxidation reaction. *ACS Omega* **2021**, *6*, 19419–19426. [[CrossRef](#)] [[PubMed](#)]
15. Nasir, J.A.; ur Rehman, Z.; Shah, S.N.A.; Khan, A.; Butler, I.S.; Catlow, C.R.A. Recent developments and perspectives in CdS-based photocatalysts for water splitting. *J. Mater. Chem. A* **2020**, *8*, 20752–20780. [[CrossRef](#)]
16. Peng, L.; Shah, S.S.A.; Wei, Z. Recent developments in metal phosphide and sulfide electrocatalysts for oxygen evolution reaction. *Chin. J. Catal.* **2018**, *39*, 1575–1593.
17. Peng, X.; Yan, Y.; Jin, X.; Huang, C.; Jin, W.; Gao, B.; Chu, P.K. Recent advance and perspectives of electrocatalysts based on transition metal selenides for efficient water splitting. *Nano Energy* **2020**, *78*, 105234. [[CrossRef](#)]
18. Hu, Y.; Mao, L.; Guan, X.; Tucker, K.A.; Xie, H.; Wu, X.; Shi, J. Layered perovskite oxides and their derivative nanosheets adopting different modification strategies towards better photocatalytic performance of water splitting. *Renew. Sustain. Energy Rev.* **2020**, *119*, 109527. [[CrossRef](#)]
19. Gershinsky, Y.; Zitoun, D. Direct chemical synthesis of lithium sub-stoichiometric olivine $\text{Li}_{0.7}\text{Co}_{0.75}\text{Fe}_{0.25}\text{PO}_4$ coated with reduced graphene oxide as oxygen evolution reaction electrocatalyst. *ACS Catalysis*. **2018**, *8*, 8715–8725. [[CrossRef](#)]
20. Zhao, Z.; Lamoureux, P.S.; Kulkarni, A.; Bajdich, M. Trends in oxygen electrocatalysis of 3d-layered (oxy) (hydro) oxides. *ChemCatChem* **2019**, *11*, 3423–3431. [[CrossRef](#)]
21. Iqbal, W.; Batool, M.; Hameed, A.; Abbas, S.; Nadeem, M.A. Boosting the activity of FeOOH via integration of ZIF-12 and graphene to efficiently catalyze the oxygen evolution reaction. *Int. J. Hydrogen Energy* **2021**, *46*, 25050–25059. [[CrossRef](#)]
22. Gao, M.R.; Xu, Y.F.; Jiang, J.; Zheng, Y.R.; Yu, S.H. Water oxidation electrocatalyzed by an efficient $\text{Mn}_3\text{O}_4/\text{CoSe}_2$ nanocomposite. *J. Am. Chem. Soc.* **2012**, *134*, 2930–2933. [[CrossRef](#)] [[PubMed](#)]
23. Pope, M.T. *Heteropoly and Isopoly Oxometalates*; Springer: Berlin/Heidelberg, Germany, 1983.
24. Dolbecq, A.; Dumas, E.; Mayer, C.R.; Mialane, P. Hybrid organic–inorganic polyoxometalate compounds: From structural diversity to applications. *Chem. Rev.* **2010**, *110*, 6009–6048. [[CrossRef](#)]
25. Sartorel, A.; Carraro, M.; Scorrano, G.; De Zorzi, R.; Geremia, S.; McDaniel, N.D.; Bernhard, S.; Bonchio, M. Polyoxometalate embedding of a tetraruthenium(IV)-oxo-core by template-directed metalation of $[\gamma\text{-SiW}_{10}\text{O}_{36}]^{8-}$: A totally inorganic oxygen-evolving catalyst. *J. Am. Chem. Soc.* **2008**, *130*, 5006–5007. [[CrossRef](#)]
26. Geletii, Y.V.; Botar, B.; Kögerler, P.; Hillesheim, D.A.; Musaev, D.G.; Hill, C.L. An all-inorganic, stable, and highly active tetraruthenium homogeneous catalyst for water oxidation. *Angew. Chem. Int. Ed.* **2008**, *47*, 3896–3899. [[CrossRef](#)]
27. Lv, H.; Geletii, Y.V.; Zhao, C.; Vickers, J.W.; Zhu, G.; Luo, Z.; Song, J.; Lian, T.; Musaev, D.G.; Hill, C.L. Polyoxometalate water oxidation catalysts and the production of green fuel. *Chem. Soc. Rev.* **2012**, *41*, 7572–7589. [[CrossRef](#)]
28. Irfan, U.; Munir, A.; Haider, A.; Ullah, N.; Hussain, I. Supported polyoxometalates as emerging nanohybrid materials for photochemical and photoelectrochemical water splitting. *Nanophotonics* **2021**, *10*, 1595–1620.
29. Li, N.; Liu, J.; Dong, B.X.; Lan, Y.Q. Polyoxometalate-based compounds for photo- and electrocatalytic applications. *Angew. Chem. Int. Ed.* **2020**, *59*, 20779–20793. [[CrossRef](#)]
30. Weakley, T.J.R.; Evans, H.T.; Showell, J.S.; Tourné, G.F.; Tourné, C.M. 18-Tungstotetracobalto(II)diphosphate and related anions: A novel structural class of heteropolyanions. *J. Chem. Soc. Chem. Commun.* **1973**, *4*, 139–140. [[CrossRef](#)]
31. Yin, Q.; Tan, J.M.; Besson, C.; Geletii, Y.V.; Musaev, D.G.; Kuznetsov, A.E.; Luo, Z.; Hardcastle, K.I.; Hill, C.L. A Fast Soluble Carbon-Free Molecular Water Oxidation Catalyst Based on Abundant Metals. *Science* **2010**, *328*, 342–345. [[CrossRef](#)]
32. Huang, Z.; Luo, Z.; Geletii, Y.V.; Vickers, J.W.; Yin, Q.; Wu, D.; Hou, Y.; Ding, Y.; Song, J.; Musaev, D.G.; et al. Efficient light-driven carbon-free cobalt-based molecular catalyst for water oxidation. *J. Am. Chem. Soc.* **2011**, *133*, 2068–2071. [[CrossRef](#)] [[PubMed](#)]
33. Stracke, J.J.; Finke, R.G. Electrocatalytic water oxidation beginning with the cobalt polyoxometalate $[\text{Co}_4(\text{H}_2\text{O})_2(\text{PW}_9\text{O}_{34})_2]^{10-}$: Identification of heterogeneous CoO_x as the dominant catalyst. *J. Am. Chem. Soc.* **2011**, *133*, 14872–14875. [[CrossRef](#)] [[PubMed](#)]
34. Natali, M.; Berardi, S.; Sartorel, A.; Bonchio, M.; Campagna, S.; Scandola, F. Is $[\text{Co}_4(\text{H}_2\text{O})_2(\alpha\text{-PW}_9\text{O}_{34})_2]^{10-}$ a genuine molecular catalyst in photochemical water oxidation? *Answers from time-resolved hole scavenging experiments Chem. Commun.* **2012**, *48*, 8808–8810.
35. Zhu, G.; Geletii, Y.V.; Kögerler, P.; Schilder, H.; Song, J.; Lense, S.; Zhao, C.; Hardcastle, K.I.; Musaev, D.G.; Hill, C.L. Water oxidation catalyzed by a new tetracobalt-substituted polyoxometalate complex: $[\{\text{Co}_4(\mu\text{-OH})(\text{H}_2\text{O})_3\}(\text{Si}_2\text{W}_{19}\text{O}_{70})]^{11-}$. *Dalton Trans.* **2012**, *41*, 2084–2090. [[CrossRef](#)]
36. Vickers, J.W.; Lv, H.; Sumliner, J.M.; Zhu, G.; Luo, Z.; Musaev, D.G.; Geletii, Y.V.; Hill, C.L. Differentiating homogeneous and heterogeneous water oxidation catalysis: Confirmation that $[\text{Co}_4(\text{H}_2\text{O})_2(\alpha\text{-PW}_9\text{O}_{34})_2]^{10-}$ is a molecular water oxidation catalyst. *J. Am. Chem. Soc.* **2013**, *135*, 14110–14118. [[CrossRef](#)]
37. Stracke, J.J.; Finke, R.G. Water Oxidation Catalysis Beginning with $\text{Co}_4(\text{H}_2\text{O})_2(\text{PW}_9\text{O}_{34})_2^{10-}$ When driven by the chemical oxidant ruthenium(III)tris(2,2'-bipyridine): Stoichiometry, kinetic, and mechanistic studies en route to identifying the true catalyst. *ACS Catal.* **2014**, *4*, 79–89. [[CrossRef](#)]
38. Stracke, J.J.; Finke, R.G. Water oxidation catalysis beginning with 2.5 μM $[\text{Co}_4(\text{H}_2\text{O})_2(\text{PW}_9\text{O}_{34})_2]^{10-}$: Investigation of the true electrochemically driven catalyst at ≥ 600 mV overpotential at a glassy carbon electrode. *ACS Catal.* **2013**, *3*, 1209–1219. [[CrossRef](#)]
39. Schiwon, R.; Klingan, K.; Dau, H.; Limberg, C. Shining light on integrity of a tetracobalt-polyoxometalate water oxidation catalyst by X-ray spectroscopy before and after catalysis. *Chem. Commun.* **2014**, *50*, 100–102. [[CrossRef](#)] [[PubMed](#)]

40. Lv, H.; Song, J.; Geletii, Y.V.; Vickers, J.W.; Sumliner, J.M.; Musaev, D.G.; Kögerler, P.; Zhuk, P.F.; Bacsa, J.; Zhu, G.; et al. An exceptionally fast homogeneous carbon-free cobalt-based water oxidation catalyst. *J. Am. Chem. Soc.* **2014**, *136*, 9268–9271. [[CrossRef](#)]
41. Goberna-Ferrón, S.; Soriano-López, J.; Galán-Mascarós, J.R.; Nyman, M. Solution speciation and stability of Cobalt-polyoxometalate water oxidation catalysts by X-ray scattering. *Eur. J. Inorg. Chem.* **2015**, *2015*, 2833–2840. [[CrossRef](#)]
42. Soriano-López, J.; Musaev, D.G.; Hill, C.L.; Galán-Mascarós, J.R.; Carbó, J.J.; Poblet, J.M. Tetracobalt-polyoxometalate catalysts for water oxidation: Key mechanistic details. *J. Catal.* **2017**, *350*, 56–63. [[CrossRef](#)]
43. Folkman, S.J.; Soriano-Lopez, J.; Galán-Mascarós, J.R.; Finke, R.G. Electrochemically driven water-oxidation catalysis Beginning with six exemplary cobalt polyoxometalates: Is it molecular, homogeneous catalysis or electrode-bound, heterogeneous CoO_x catalysis. *J. Am. Chem. Soc.* **2018**, *140*, 12040–12055. [[CrossRef](#)]
44. Arens, J.T.; Blasco-Ahicart, M.; Azmani, K.; Soriano-López, J.; García-Eguizábal, A.; Poblet, J.M.; Galán-Mascarós, J.R. Water oxidation electrocatalysis in acidic media with Co-containing polyoxometalates. *J. Catal.* **2020**, *389*, 345–351. [[CrossRef](#)]
45. Gong, R.; Gao, D.; Liu, R.; Sorsche, D.; Biskupek, J.; Kaiser, U.; Rau, S.; Streb, C. Self-activation of a polyoxometalate-derived composite electrocatalyst for the oxygen evolution reaction. *ACS Appl. Energy Mater.* **2021**, *4*, 12671–12676.
46. Azmani, K.; Besora, M.; Soriano-López, J.; Landolsi, M.; Teillout, A.L.; de Oliveira, P.; Mbomekall'e, I.M.; Poblet, J.M.; Galán-Mascarós, J.R. Understanding polyoxometalates as water oxidation catalysts through iron vs. cobalt reactivity. *Chem. Sci.* **2021**, *12*, 8755–8766. [[CrossRef](#)]
47. Ahmed, T.; Asghar, M.A.; Ali, A.; Akhter, Z.; Ali, S.; Ullah, I.; Nisar, T.; Wagner, V.; Touseef, S.; Hussain, A.; et al. High-nuclearity cobalt(II)-containing polyoxometalate anchored on nickel foam as electrocatalyst for electrochemical water oxidation studies. *J. Alloys Compd.* **2022**, *909*, 164709. [[CrossRef](#)]
48. Thostenson, E.T.; Li, W.Z.; Wang, D.Z.; Ren, Z.F.; Chou, T.W. Carbon nanotube/carbon fiber hybrid multiscale composites. *J. Appl. Phys.* **2002**, *91*, 6034–6037. [[CrossRef](#)]
49. Sharma, M.; Gao, S.; Mäder, E.; Sharma, H.; Wei, L.Y.; Bijwe, J. Carbon fiber surfaces and composite interphases. *Compos. Sci. Technol.* **2014**, *102*, 35–50. [[CrossRef](#)]
50. Ali, A.; Shah, S.M.; Bozar, S.; Kazici, M.; Keskin, B.; Kaleli, M.; Akyürekli, S.; Günes, S. Metal-free polymer/MWCNT composite fiber as an efficient counter electrode in fiber shape dye-sensitized solar cells. *Nanotechnology* **2016**, *27*, 384003. [[CrossRef](#)] [[PubMed](#)]
51. Ali, A.; Akyuz, D.; Asghar, M.A.; Koca, A.; Keskin, B. Free-standing carbon nanotubes as non-metal electrocatalyst for oxygen evolution reaction in water splitting. *Int. J. Hydrogen Energy* **2018**, *43*, 1123–1128. [[CrossRef](#)]
52. Lekawa-Raus, A.; Patmore, J.; Kurzepa, L.; Bulmer, J.; Koziol, K. Electrical properties of carbon nanotube based fibers and their future use in electrical wiring. *Adv. Funct. Mater.* **2014**, *24*, 3661–3682. [[CrossRef](#)]
53. Chhetri, K.; Muthurasu, A.; Dahal, B.; Kim, T.; Mukhiya, T.; Chae, S.-H.; Ko, T.H.; Choi, Y.C.; Kim, H.Y. Engineering the abundant heterointerfaces of integrated bimetallic sulfide-coupled 2D MOF-derived mesoporous CoS₂ nanoarray hybrids for electrocatalytic water splitting. *Mater. Today Nano* **2022**, *17*, 100146. [[CrossRef](#)]
54. Kandel, M.R.; Pan, U.N.; Paudel, D.R.; Dhakal, P.P.; Kim, N.H.; Lee, J.H. Hybridized bimetallic phosphides of Ni-Mo, Co-Mo, and Co-Ni in a single ultrathin-3D-nanosheets for efficient HER and OER in alkaline media. *Compos. B Eng.* **2022**, *239*, 109992. [[CrossRef](#)]
55. Suen, N.T.; Hung, S.F.; Quan, Q.; Zhang, N.; Xu, Y.J.; Chen, H.M. Electrocatalysis for the oxygen evolution reaction: Recent development and future perspectives. *Chem. Soc. Rev.* **2017**, *46*, 337–365. [[CrossRef](#)]
56. Jiao, Y.; Zheng, Y.; Jaroniec, M.; Qiao, S.Z. Design of electrocatalysts for oxygen-and hydrogen-involving energy conversion reactions. *Chem. Soc. Rev.* **2015**, *44*, 2060–2086. [[CrossRef](#)] [[PubMed](#)]
57. Kang, Z.; Wang, E.; Mao, B.; Su, Z.; Gao, L.; Lian, S.; Xu, L. Controllable fabrication of carbon nanotube and nanobelt with a polyoxometalate-assisted mild hydrothermal process. *J. Am. Chem. Soc.* **2005**, *127*, 6534–6535. [[CrossRef](#)] [[PubMed](#)]
58. Grewe, T.; Deng, X.; Tüysüz, X. Influence of Fe doping on structure and water oxidation activity of nanocast Co₃O₄. *Chem. Mater.* **2014**, *26*, 3162–3168. [[CrossRef](#)]
59. Sivanantham, A.; Ganesan, P.; Shanmugam, S. Hierarchical NiCo₂S₄ nanowire arrays supported on Ni foam: An efficient and durable bifunctional electrocatalyst for oxygen and hydrogen evolution reactions. *Adv. Funct. Mater.* **2016**, *26*, 4661–4672. [[CrossRef](#)]
60. Luo, W.; Hu, J.; Diao, H.; Schwarz, B.; Streb, C.; Song, Y.F. Robust polyoxometalate/nickel foam composite electrodes for sustained electrochemical oxygen evolution at high pH. *Angew. Chem. Int. Ed.* **2017**, *56*, 4941–4944. [[CrossRef](#)] [[PubMed](#)]
61. Tantraviwat, D.; Anuchai, S.; Ounnunkad, K.; Saipanya, S.; Aroonyadet, N.; Rujijanagul, G.; Inceesungvorn, B. Structural properties of tungsten-doped cobalt molybdate and its application in electrochemical oxygen evolution reaction. *J. Mater. Sci. Mater. Electron.* **2018**, *29*, 13103–13111. [[CrossRef](#)]
62. Zhang, L.; Ding, X.; Cong, M.; Wang, Y.; Zhang, X. Self-adaptive amorphous Co₂P@Co₂P/Co-polyoxometalate/nickel foam as an effective electrode for electrocatalytic water splitting in alkaline electrolyte. *Int. J. Hydrog. Energy* **2019**, *44*, 9203–9209. [[CrossRef](#)]
63. Wang, Y.; Wang, Y.; Zhang, L.; Liu, C.S.; Pang, H. Core-shell-type ZIF-8@ZIF-67@POM hybrids as efficient electrocatalysts for the oxygen evolution reaction. *Inorg. Chem. Front.* **2019**, *6*, 2514–2520. [[CrossRef](#)]
64. Li, Q.Y.; Zhang, L.; Xu, Y.X.; Li, Q.; Xue, H.; Pang, H. Smart yolk/shell ZIF-67@POM hybrids as efficient electrocatalysts for the oxygen evolution reaction. *ACS Sustain. Chem. Eng.* **2019**, *7*, 5027–5033. [[CrossRef](#)]

-
65. Wang, Y.; Wang, Y.; Zhang, L.; Liu, C.S.; Pang, H. PBA@ POM hybrids as efficient electrocatalysts for the oxygen evolution reaction. *Chem.: Asian J.* **2019**, *14*, 2790–2795.
 66. Park, K.R.; Jeon, J.E.; Ali, G.; Ko, Y.H.; Lee, J.; Han, H.; Mhin, S. Oxygen evolution reaction of Co-Mn-O electrocatalyst prepared by solution combustion synthesis. *Catalysts* **2019**, *9*, 564. [[CrossRef](#)]